Earthquakes triggered by the subsurface undrained response to reservoir impoundment at Irapé, Brazil

Haris Raza[1,2,3]**, George Sand França**[1,2]**, Eveline Sayão**[1]**, and Victor Vilarrasa**[3]

[1]Seismological Observatory, Graduate Program in Geology, Institute of Geosciences, University of Brasília,
Campus Darcy Ribeiro, 70297-400 Brasília, Brazil
[2]Institute of Astronomy, Geophysics and Atmospheric Sciences, University of São Paulo, 05508-090 São Paulo, Brazil
[3]Global Change Research Group (GCRG), IMEDEA, CSIC-UIB, 07190 Esporles, Spain

Correspondence: Haris Raza (harisraza90@yahoo.com) and Victor Vilarrasa (victor.vilarrasa@csic.es)

Abstract. The necessity to reduce carbon emissions to mitigate climate change is accelerating the transition from fossil fuels to renewable energy sources. Specifically, hydropower has emerged as a prominent and safe renewable energy source but entails reservoir-triggered seismicity (RTS). This phenomenon causes significant challenges for safe reservoir management. Irapé, in Brazil, is a prominent RTS site where seismicity surged after reservoir filling, with a maximum event of magnitude 3.0 in May 2006, just 6 months after the start of reservoir impoundment. Despite the fact that more than 1 decade has passed since the seismicity occurred, the factors governing these earthquakes and their connection to subsurface rock properties remain poorly understood. Here, we attempt to understand the potential causes of RTS at Irapé Dam, which is the highest dam in Brazil at 208 m and the second highest in South America. Permeability and porosity measurements of cylindrical cores from hard and intact rock samples, which were extracted near the RTS zone by pitting 10 cm from the surface, reveal a low-permeability rock. Porosity values range from 6.3 % to 14.7 %. Only 3 out of the 11 tested samples present permeability above the lowest measurable value of the apparatus (0.002 mD), with the highest permeability being 0.0098 mD. The undrained response of the low-permeability rock placed below the reservoir results in an instantaneous increase in pore pressure and poroelastic stress changes due to elastic compression, which brings potential faults located below the reservoir closer to failure conditions. According to our analytical calculations, the vertical loading caused by the increase of 136 m in the reservoir water level led to a 0.61 MPa pore pressure buildup in response to compression at the depth of the M_{w} 3.0 earthquake, i.e., 3.88 km, resulting in an increase of 0.75 MPa in the vertical effective stress and of 0.48 MPa in the horizontal effective stress. These changes resulted in an increase in the deviatoric stress that led to fault destabilization, causing the RTS. The laboratory measurements and analytical calculations corroborate the hypothesis that the initial seismic activity was induced by the undrained subsurface response to the reservoir loading at Irapé.

1 Introduction

Reservoir impoundment, deep underground mining, and fluid injection into and withdrawal from the subsurface are some of the well-known causes of induced/triggered seismicity which have become a global issue in the past few decades (McGarr et al., 2002; Foulger et al., 2018; Kivi et al., 2023). The understanding and identification of these types of human-induced earthquakes is crucial in terms of environmental and economic impact and for socio-political and scientific discussion (González et al., 2012; Vilarrasa et al., 2019). Recently, the debate over the potential induced or triggered nature of cases of felt seismicity has intensified, such as the Oklahoma earthquakes of M_{w} 5.7 in 2011 and M_{w} 5.8 in 2016 (Ellsworth, 2013; Keranen et al., 2013; Yeck et al., 2016); the earthquakes in Emilia, Italy, of M_{w} 6.1 and 5.9 in 2012 (Cesca et al., 2013); the earthquake in Pohang, South Korea, of M_{w} 5.5 in 2017 (Grigoli et al., 2018; Kim et al., 2018); the earthquake in Lorca, Spain, of M_{w} 5.1 in 2011

(González et al., 2012); and the earthquake in Castor, Spain, of M_w 4.1 in 2013 (Cesca et al., 2014; Vilarrasa et al., 2021, 2022), to name a few. Apart from the possibility of injuring people and damaging infrastructure, such earthquakes can have a negative public perception leading to project cancellation (Boyet et al., 2023a).

The first reservoir-triggered seismicity (RTS) case was observed during the filling of Lake Mead at the Hoover Reservoir (US) in the mid-1930s, with $\sim M_{4.0}$ (Carder, 1945). Major worldwide RTS cases were detected in the 1960s, such as $M_{6.1}$ in Hsinenghiang (China) in 1962, $M_{6.2}$ in Kariba (Zambia) in 1963, $M_{6.3}$ in Kremasta (Greece) in 1966, and $M_{6.3}$ in Koyna (India) in 1967 (Gupta, 2002). To date, over 150 RTS cases have been documented (Wilson et al., 2017; Foulger et al., 2018). Studies to understand the triggering mechanisms of RTS show that pore pressure changes in the order of a few 10ths of MPa and the associated poroelastic stress changes are sufficient to reactivate deep faults (Rice and Cleary, 1976; Simpson, 1976; Bell and Nur, 1978; Talwani and Acree, 1985; Roeloffs, 1988; Simpson et al., 1988).

RTS is generally controlled by the stress state, the geological and hydrogeological properties of the region, and the water level changes at the reservoir. The perturbation caused by the changes in water level results in the loading and/or unloading of the subsurface, which may respond in a drained or undrained way. An undrained response leads to an instantaneous pore pressure buildup that is proportional to the height of the reservoir load. In contrast, a drained response leads to pore pressure diffusion into the rock that causes progressive pore pressure buildup as the pressure front propagates into the rock (Table 1). In general, RTS magnitudes are smaller for undrained responses than drained ones (Simpson et al., 1988). The interactions and comprehensive analysis of these two responses are key to understanding the causes of RTS cases and eventually improve the forecasting and mitigation of RTS hazard.

The RTS cases are booming around the world, with Brazil being one of the concerned countries, with 29 RTS cases to date (Sayão et al., 2020). The study of RTS in Brazil started in 1972 with the $M_{3.7}$ at Carmo do Cajuru reservoir, southeastern Brazil (Foulger et al., 2018). The largest recorded event, an $M_{4.2}$ in 1974, caused damage to several buildings without any fatalities and was associated with nearby reservoirs at Porto Colombia and Volta Grande, both of which started damming in the early 1970s (Sayão et al., 2020).

Irapé Dam, located in the state of Minas Gerais, Brazil, is the highest dam in Brazil at about 208 m and the second highest in South America (França et al., 2010). The Irapé hydropower plant lies in the vicinity of the Jequitinhonha River. Seismicity started to increase immediately after the impoundment of the reservoir and completion of the dam, with the maximum event of $M_{3.0}$ occurring on 14 May 2006, coinciding with the peak water level of the dam. The significant magnitude of the earthquake and the early occurrence after filling the reservoir impoundment has raised questions about the triggering mechanisms of this RTS. Understanding these mechanisms is crucial for ensuring the safety of infrastructure around the Irapé reservoir and for the local population.

In this study, we aim to investigate the potential causes of the main RTS event at Irapé. We initially elaborate on the geological setting and rock characteristics in the vicinity of the reservoir. We explain the characteristics of the RTS at Irapé, including the temporal evolution of the seismicity, which occurred in the short period from December 2005 to May 2006, and the location of the main event based on the local velocity model. Then, we present the performed permeability and porosity tests of cylindrical cores from hard and intact rock samples, which were extracted near the RTS zone to identify and describe the primary role of porosity and permeability. We perform analytical calculations to estimate the pore pressure and poroelastic stresses in response to the highest water level of the reservoir filling and the time it would take for the pore pressure diffusion front to reach the depth of the main event. We present evidence that the cause of RTS at Irapé was the undrained response of the subsurface to reservoir impoundment.

2   Geological setting and RTS at Irapé

2.1   Geological setting

The area of Irapé is located within the domain of the pre-folding Cambrian Araçuaí Belt, which is oriented approximately in a north–south direction and defines the eastern part of the São Francisco Craton in the state of Minas Gerais (Almeida, 1977). Approximately 80 % of the reservoir area in Irapé corresponds to the Chapada Acauã Formation. The Chapada Acauã Formation, which has been investigated near the Irapé shear zone (Araujo Filho et al., 2010), consists of carbonaceous mica schist rocks, with pyrite, garnet, or graphite locally (Lima et al., 2002). This rock is intensely deformed, characterized by the formation and rotation of quartz sub-grains and the migration of grain edges (Araujo Filho et al., 2010). This formation is characterized by typical passive margin sedimentation and is associated with sediment deposition in the Macaúbas Basin along with the Nova Aurora Formation (Silva et al., 2014). The Ribeirão da Folha Formation is found to the east of the Chapada Acauã Formation, consisting of mica shales, quartzite, and calc–silicate rock (Fig. 1).

2.2   Background on the reservoir-triggered seismicity at Irapé

The Irapé reservoir covers an area of 137.8 km^2 with a reservoir volume of 5.964 km^3. The dam was constructed on the Jequitinhonha River, filling the reservoir to a maximum height of 137 m (Fig. 1 and Table 2). The dam area was monitored by a three-component seismic network at three stations

Table 1. The time distribution types of responses to reservoir-triggered earthquakes by Simpson (1988).

Response type	Mechanism	Description	Main features	Cases
Instantaneous response	Instantaneous elastic response and undrained response due to reservoir loading	This type of RTS increases immediately after the initial impoundment of the reservoir or changes rapidly after rapid changes in the water level.	Changes in water level have a strong correlation with the change in seismicity. This generally occurs around the reservoir area, and the earthquake magnitude is small; the majority of them are swarm seismicity.	Koyna, Monticello, Manico-3, Nurek, Kariba, Kremesta Irapé (this paper)
Delayed response	Increase in pore pressure caused by pressure diffusion through permeable rock below the reservoir	It is only after a period of reservoir impoundment that the seismicity changes continuously.	There is no significant correlation between changes in water level and seismicity, the time delay is obvious, the magnitude is generally large, and the earthquake occurrence point is not limited.	Koyna, Aswan, Oroville
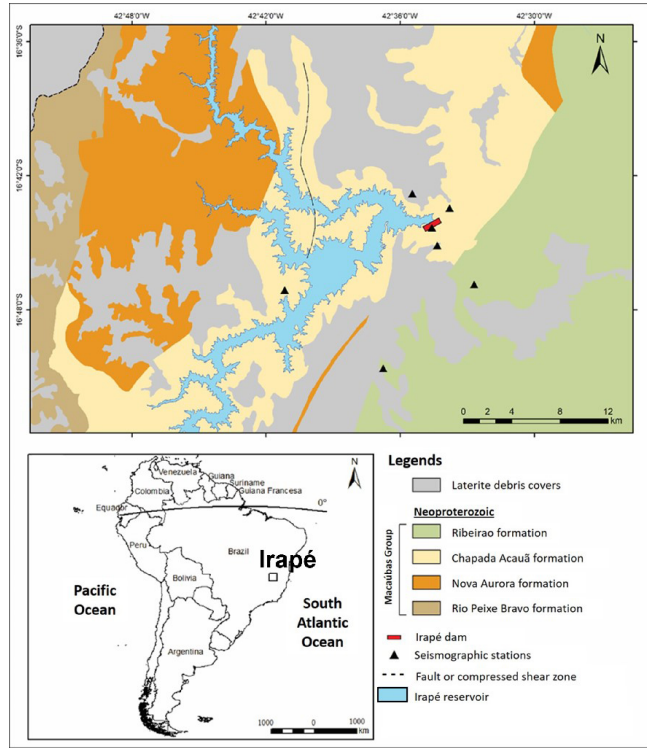
Figure 1. Geological map of Irapé reservoir and surrounding area.

Figure 2. Temporal evolution of RTS at Irapé over 10 d. The number of events during December 2005 to May 2006 (histogram) at Irapé and the average water elevation above the mean sea level (blue line) are illustrated. The red star indicates the time when the main and largest event occurred, $M_{3.0}$ on 14 May 2006 (modified from Silva et al., 2014).

prior to 3 years of its impoundment, which started on 7 December 2005. These stations did not detect any seismicity before the impoundment (Chimpliganond et al., 2007).

Microearthquakes started to be detected just 1 d after the impoundment began, exceeding 300 microearthquakes by October 2006. The largest event occurred on 14 May 2006 with an $M_{3.0}$ that was felt at the reservoir area at a depth of 3.88 km (Chimpliganond et al., 2007; França et al., 2010). The seismicity occurred within a small area, with epicenters in the lake and its nearby margins (less than 3 km from the narrow lake), close to the dam axis. The epicenters are dis-

tributed from 0 to 11.4 km depth, showing a progressive increase in depth (see Table S1). The evident temporal correlation between the start of the reservoir impoundment and the occurrence of seismicity leads us to investigate a causative relationship (Figs. 2 and 3). The spatial distribution of the epicenters also suggests the hypothesis that this is another case of RTS of the initial response type.

The events were analyzed using the program Seismic Analysis Code (Goldstein and Snoke, 2005), in which the arrival of the P and S waves and the polarity are considered. The hypocenter location of the events that were recorded by three stations was computed with the program HYPO71 (Lee and Lahr, 1975). The analysis of seismograms went through a double-checks routine (Silva et al., 2014). The local monitoring station presented operational challenges, which resulted in positional uncertainty in seismic events (Silva et al., 2014). The velocity model that was used to locate the seismic events was based on a deep seismic refraction survey in combination

Table 2. Characteristics of the main RTS event at Irapé (França et al., 2010).

Dam height (m)	Length (m)	Volume (km^3)	Max. reservoir water depth (m)	Reservoir area (km^2)	Seismicity type	Date	Magnitude (mR)	Io (MMI)	ΔT (yr)
208	540	5.964	137	137.8	Initial	14 May 2006	3.0	III–IV	0.5

ΔT: time interval (years) since the start of filling/impoundment; MMI: Modified Mercalli Intensity scale; mR: regional magnitude.
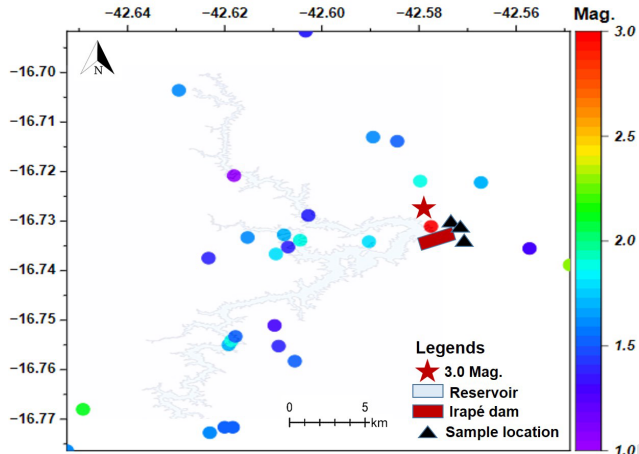
Figure 3. RTS distribution in the initial period with location and magnitude (see color scale). The red star is the main event felt near the dam, and black triangles denote the sample location.

with local geological interpretations and studies of the crustal structure in southeastern Brazil (Assumpção et al., 2002).

Velocity models were adopted based on a deep seismic refraction survey in combination with local geological interpretations and studies of the crustal structure in southeastern Brazil to locate seismic events in the Irapé area (Assumpção et al., 2012). The local velocity model consists of a superficial 4.8 km thick layer with a P-wave velocity (V_p) of 4.5 km s^{-1}, representing the mica schist to graphite schist rocks from surface, and a second layer from schist to crystalline basement rocks with a thickness of 11.2 km with P-wave velocity (V_p) of 6 km s^{-1} (Marshak et al., 2006; Silva et al., 2014).

The repetition of a structural trend in the NE–SW direction originates from the geological and geophysical structuring of the crust (Silva et al., 2014). The stress regime in the Irapé region has been estimated to be a normal faulting stress regime. The accuracy of the focal mechanisms remains a subject of debate due to the low quality of the seismic data recorded by analog seismograms and uncertainties associated with the velocity model. Consequently, the focal mechanisms of the $M_{3.0}$ earthquake on 14 May 2006 have not been resolved yet (Silva et al., 2014).

3 Materials and methodology

We inspected the Irapé site and surrounding areas, as well as the outcrops. The dam area is surrounded by mica schist rock, which is shiny, ranging from blackish to medium gray in color, with foliated, fine- to medium-grained textures. According to the local velocity model, there is a superficial layer that is 4.8 km thick, representing mica schist to graphite schist rocks at the surface. Below that, there is a second layer that is 11.2 km thick, consisting of crystalline basement rock. Measurements from these samples are crucial for understanding the estimated permeability beneath the subsurface in the context of the main event, which occurred at a depth of 3.88 km (França et al., 2010). Since the epicenter of the main event was located about 1 km away from the dam, we collected bulk rock samples from different locations around the dam and nearby outcrops by digging pits that were 0.10 m deep.

3.1 Laboratory experiments

We extracted cylindrical core samples perpendicular to the bedding planes of mica schist rock. We performed tests on three sets of samples, with a total of 11 core samples, which were hard and intact samples because the rest of the samples were fragile and fractured during the coring from bulk samples (Table 3). The retrieved cylindrical plugs had a length ranging from 3.8 to 5.0 cm and a diameter of 2.50 cm, which meets the international standard criteria (Core Lab) to measure core plug samples with Ultra-Pore 300 and Ultra-Perm 610 (Fig. 4).

We conducted porosity measurements using the Ultra-Pore 300, which is manufactured by Core Lab Instruments in Texas, USA. The Ultra-Pore 300 is a gas expansion helium pycnometer specifically designed for determining the grain volume or pore volume of both core plug and full-diameter samples. To achieve this, we utilized matrix cups designed for samples with diameters ranging from 2.5 to 3.8 cm, equipped with a Setra 204 transducer rated for pressures ranging from 0 to 1.72 MPa. We determined the pore volume using the nitrogen gas (N$_2$) expansion technique (API, 1998; Ceia et al., 2019).

We measured the intrinsic permeability of rock samples using Ultra-Perm 610 Permeameter. This precision equipment, which controls back-pressure, maintains a constant rate or mean pressure at 0.69 MPa. Before testing, samples

Table 3. Location of samples with permeability and porosity data from measured cores.

Location (lat., long.)	Sample numbers	Permeability (mD)	Porosity (%)
16.73872, 42.57680	IR-1a	< 0.002	7.5
	IR-1b	< 0.002	6.8
	IR-1c	< 0.002	8.8
	IR-1d	0.0098	6.6
16.74038, 42.57652	IR-2a	< 0.002	9.5
	IR-2b	0.0038	10.5
	IR-2c	0.0038	14.7
16.72438, 42.56316	IR-3a	< 0.002	6.9
	IR-3b	< 0.002	13.3
	IR-3c	< 0.002	7.1
	IR-3d	< 0.002	6.3

Experiments loaded perpendicular to bedding plane ($\perp$).
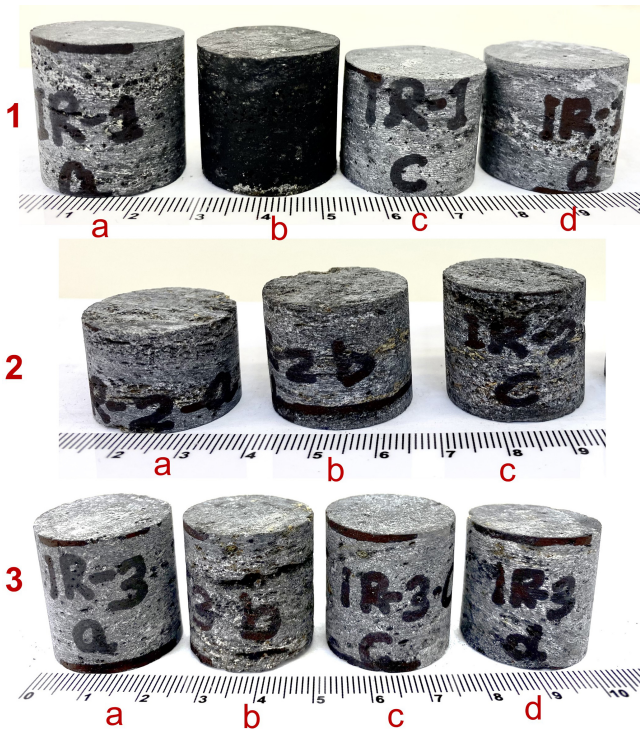
Figure 4. The three sets of mica schist rock samples (1, 2, and 3) after cylindrical coring from bulk samples ($\perp$ coring of cylindrical plugs was done by loading perpendicular to the bedding planes).

were cleaned with Soxhlet equipment and toluene, followed by drying in an oven. The permeability measurements included a permeameter, a nitrogen source, a stopwatch, a core holder, a bubble tube, and a digital calliper. The core holder was pressurized to 3.45 MPa confining pressure using compressed air. The bubbles passing through a burette were timed, and outflow gas volume was recorded. The per-

meability was calculated using Darcy's law, considering core dimensions. Hard rock core samples, like mica schist, require long stabilization times due to the low permeability.

3.2 Analytical calculations of undrained pore pressure and stress changes

Reservoir impoundment causes an undrained effect in the subsurface that manifests as instantaneous pore pressure and stress changes below the reservoir (Skempton, 1954). The change in the vertical stress, $\Delta\sigma_{\mathrm{v}}$, equals the weight of the water level rise assuming an extensive reservoir. The horizontal stress, assuming oedometric conditions, changes as follows because of the increase in the vertical stress and the undrained pore pressure change (Rutqvist, 2012):

$$\Delta\sigma_h = \frac{\nu}{(1-\nu)}\left(\Delta\sigma_{\mathrm{v}}\right) + \alpha\frac{(1-2\nu)}{(1-\nu)}\Delta p, \qquad (1)$$

where $\Delta\sigma_{\mathrm{h}}$ is the horizontal stress change, α is Biot's coefficient, ν is Poisson's ratio, and Δp is the pore pressure change. Additionally, in an isotropic and homogeneous poroelastic material subject to undrained conditions, the change in pore pressure resulting from a change in stress can be computed as follows (e.g., Rice and Cleary, 1976; Cocco and Rice, 2002):

$$\Delta p = \frac{B}{3}\Delta\sigma_{\mathrm{kk}}, \qquad (2)$$

where $\Delta\sigma_{\mathrm{kk}} = \Delta\sigma_{\mathrm{v}} + 2\Delta\sigma_{\mathrm{h}}$, $\Delta\sigma_{\mathrm{kk}}$ is the mean stress change, and B is Skempton's coefficient of mica schist rock (Roeloffs, 1988). Here we adopt the sign criterion of geomechanics; i.e., compressive stresses are positive. Equations (1) and (2) constitute a system of two equations with two unknowns. Their resolution yields the undrained pore pressure
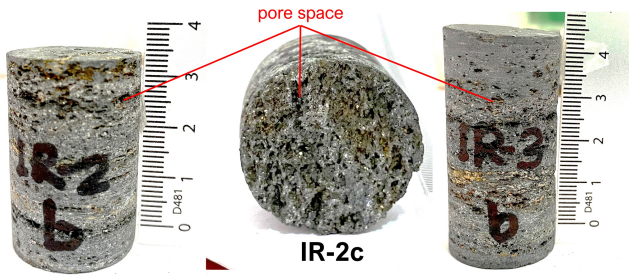
Figure 5. Megascopic representation of samples IR-2b and c and IR-3b showing pores that are not well connected.

change as

$$\Delta p = \frac{B}{3} \frac{(1+\nu)\,\Delta\sigma_{\mathrm{v}}}{\left(1-\nu-\frac{2B}{3}\left(\alpha-\nu-2\alpha\nu\right)\right)}. \tag{3}$$

3.3 Analytical calculations of the time at which the pore pressure diffusion front reaches the depth of the earthquake

The advancement of the pore pressure front within the subsurface is controlled by diffusivity:

$$D = \frac{k\rho g}{\mu S_{\mathrm{s}}}, \tag{4}$$

where D is diffusivity, k is the intrinsic permeability, ρ is water density, g is gravity, μ is water viscosity, and S_{s} is the specific storage coefficient. The time at which the pore pressure front reaches a certain distance r is given by

$$t = \frac{r^2}{D}. \tag{5}$$

4 Results

4.1 Porosity and permeability measurements

The results of our laboratory measurements are provided in Table 3. These data are subject to measurement uncertainties inherent to the experimental equipment used according to the standard procedure. Laboratory measurements of samples of mica schist reveal a low permeability (Table 3 and Fig. 6). The maximum permeability is 0.0098 mD, but most of the samples present a lowest measurable permeability value of the apparatus, i.e., 0.002 mD. Such permeability is in the range of low-permeability rock, which acts as a barrier to flow. Most of the samples have a porosity between 6 % and 10 %, except for two with higher porosity. The low permeability of mica schist could be explained by the fact that the larger pores are not well connected (Fig. 5). In general, there is no correlation between permeability and porosity (Fig. 6).
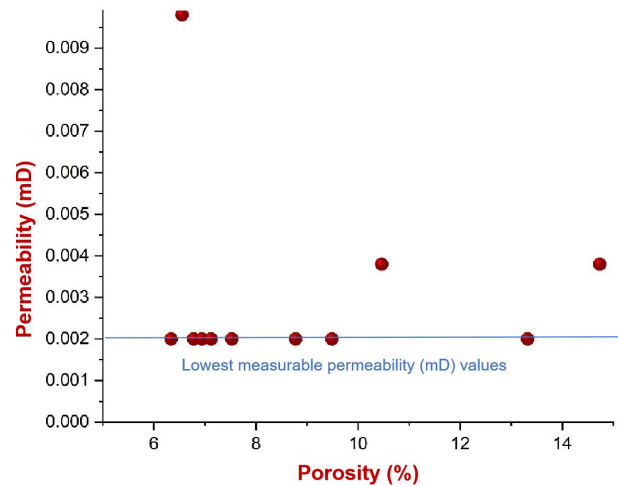
Figure 6. Porosity–permeability relation of mica schist rock samples.

4.2 Undrained response of rock: changes in pore pressure and stress

The 136 m of water level increase at the time of the $M_{3.0}$ earthquake resulted in an increase in the vertical stress of 1.36 MPa. To compute the pore pressure change caused by the reservoir impound­ment, the Biot coefficient, Skempton's B coefficient, and Poisson's ratio of mica schist are needed (Eq. 3). Since such measurements are not available, we adopt the values of Opalinus Clay because it is a similar rock to mica schist (both are shales primarily composed of quartz minerals). Thus, we assume Skempton's B coefficient of 0.92, an undrained Poisson's ratio of 0.39, and Biot's co­efficient of 1. With these values, the resulting pore pres­sure change is 0.61 MPa. Consequently, the horizontal stress change is 1.09 MPa (Eq. 1). These pore pressure and stress changes result in an increase in the vertical effective stress of 0.75 MPa and in the horizontal effective stress of 0.48 MPa, increasing the deviatoric stress by more than 0.25 MPa.

4.3 Pressure diffusion along mica schist

The measured intrinsic permeability of mica schist is in the order of 10^{-18} m^2 (Table 3). Assuming a specific storage co­efficient in the order of 1.05×10^{-6} m^{-1}, diffusivity (Eq. 4) results in 9.5×10^{-6} m^2 s^{-1}. Taking into account that the depth of the $M_{3.0}$ earthquake occurred at 3.8 km, the time at which the pore pressure front would reach this depth by diffusion (Eq. 5) is in the order of 50 000 years by assuming the absence of fractures.

5 Discussion

RTS has been the focus of many studies, but the origin and development of RTS are still unclear in many cases (Gupta

et al., 2016; Arora et al., 2018). There is a general consensus that there are two main triggering mechanisms (Simpson et al., 1988). On the one hand, low-permeability rock has an undrained response to the water level changes in the reservoir, which acts as a loading, instantaneously increasing pore pressure and causes poroelastic stress changes deep underground (Chen and Talwani, 2001; Vilarrasa et al., 2022; Raza et al., 2023; Vilarrasa et al., 2023). On the other hand, in the presence of permeable rock or a permeable fracture network, pore pressure diffuses downwards, which may eventually trigger an earthquake if a critically stressed fault becomes pressurized (Talwani and Acree, 1985).

At Irapé, the low permeability of the rock below the reservoir, i.e., mica schist with permeability in the order of $10^{-18}\,\mathrm{m}^2$ or lower, hinders pore pressure diffusion. Given that the hypocenter was located at 3.88 km depth, the pressure propagation front would take in the order of 50 000 years to start pressurizing the depth at which the earthquake was nucleated. Even assuming that the presence of fractures enhanced the rock permeability by 3 orders of magnitude, which would be the upper limit of observed permeability enhancement of low-permeability rock at the field scale (Neuzil, 1986), the pressure front would take 50 years to reach 3.88 km depth. The permeability enhancement due to the presence of fractures could become larger in crystalline than in clay-rich rock, reaching an increase of up to 5 orders of magnitude (Bondarenko et al., 2022). Such high permeability enhancement caused by fractures is not feasible in clay-rich rock like mica schist because of its ductility and low dilatancy angle, which prevent fractures from becoming open pathways. At Irapé, the necessary permeability of the rock to reach the depth of the largest earthquake within 0.5 years, i.e., the delay of the earthquake with respect to the start of impoundment, would be of $10^{-13}\,\mathrm{m}^2$, 5 orders of magnitude higher than the actual permeability of mica schist. Such high permeability enhancement is deemed unlikely for mica schist.

Considering the load caused by the water level rise in the reservoir of 136 m, the low-permeability mica schist experienced an undrained response, with subsequent poroelastic stress and pore water changes. We have estimated these changes analytically, finding a vertical effective stress increase of 0.75 MPa, a horizontal effective stress increase of 0.48 MPa, and a pore pressure increase of 0.61 MPa. Given the normal faulting stress regime at Irapé, these changes cause an increase in the deviatoric stress that could destabilize faults in the subsurface. These changes in pore pressure and stress levels provide valuable insights into the dynamic behavior of the geological formation and are crucial considerations in understanding the reservoir response to alterations in reservoir water levels. We contend that the rapid loading of the reservoir weakens this fault because of the undrained stress and pore pressure changes (Fig. 7).

In addition, the megascopic representation of core samples in the configuration of the physical evidence illustrates that rocks can exhibit relatively high porosities and low permeability when their pores are not well connected (Fig. 5). Thus, mica schist may present preferential lateral fluid migration at depth, following the foliation direction. The surface rock beneath the Irapé reservoir is highly metamorphosed, and, despite having high porosity, the rock presents low permeability. Therefore, pore pressure diffusion is disregarded as the potential cause triggering the seismicity at Irapé.

The regional geology at the eastern part of the São Francisco Craton in the state of Minas Gerais follows an N–S direction (Almeida, 1977). Silva et al. (2014) also mentioned that the repetition of a structural trend in the NE–SW direction originates from the geological and geophysical structuring of the crust. This trend makes it feasible to assume the existence of an N–S vertical mature fault that could become destabilized by small changes in the effective stress. An association of such seismicity with the shear zone along reservoir/lineaments suggests the reactivation of such faults under the influence of reservoir impoundment.

Mitigation of the risk of RTS requires knowledge of the physical mechanisms that may trigger seismicity. Thus, a thorough characterization of the site to measure rock physical properties is crucial. Analytical and numerical solutions should integrate the physics of the problem, in particular, poromechanics to assess both the undrained response of the subsurface to reservoir impoundment and pore pressure diffusion. Such models should include the rock layers below the reservoir down to the crystalline basement and their characteristics, including features like faults. Before the construction of the dam, the hazard of triggering moderate to large earthquakes should be estimated, to disregard locations with a high probability of RTS. This estimation requires knowing the hydro-mechanical properties of the rock layers, i.e., permeability, porosity, stiffness, and strength, and the design parameters of the dam, i.e., height for potential future projects. Note that, at Irapé, the porosity and permeability measurements have not been taken until now but should have been taken prior to the design of the dam. The successful management of RTS requires an interdisciplinary approach combining concepts of hydrogeology, geomechanics, and seismology.

To address and manage RTS risks, the Traffic Light Protocol (TLP) should be employed (Fig. 8). A TLP is a tool that assists decision-makers to decide how to operate the dam to minimize risks. The TLP has three levels of operation: (1) a green light that allows operations to proceed without restrictions, (2) a yellow light that requires the activation of mitigation measures, and (3) a red light that urges operations to stop. Efforts have been made regarding the incorporation of real-time data with the application of risk-oriented measures to prevent infrastructure damage and nuisance to the local community. Incorporating the two types of RTS in the TLP, i.e., immediate events induced by the undrained response of the subsurface to water level changes and delayed seismicity induced by pore pressure diffusion, is crucial. To this end, the
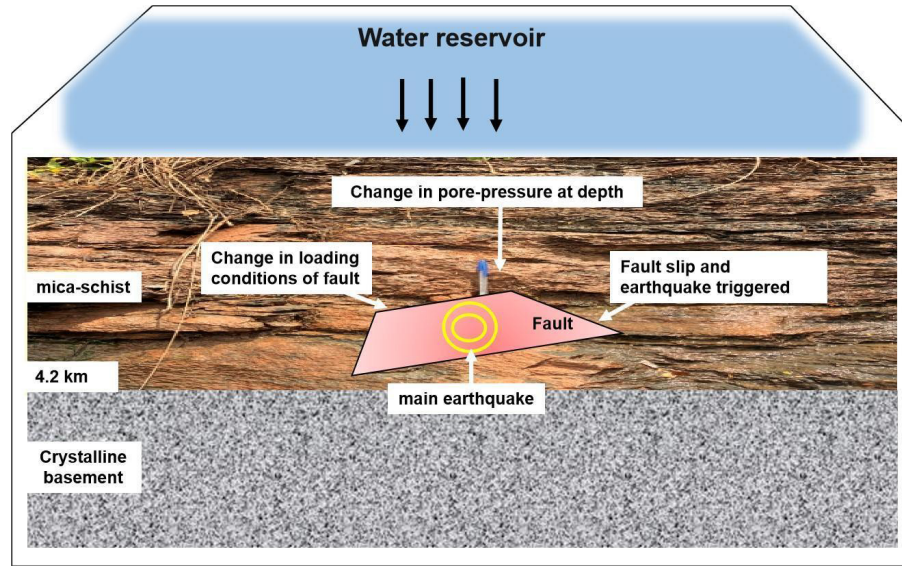
Figure 7. Schematic description of the mechanism of RTS at Irapé, indicating the effect of the weight of the reservoir water volume due to undrained response in mica schist rock of low permeability (the background photo was taken in the field from an outcrop at Irapé).
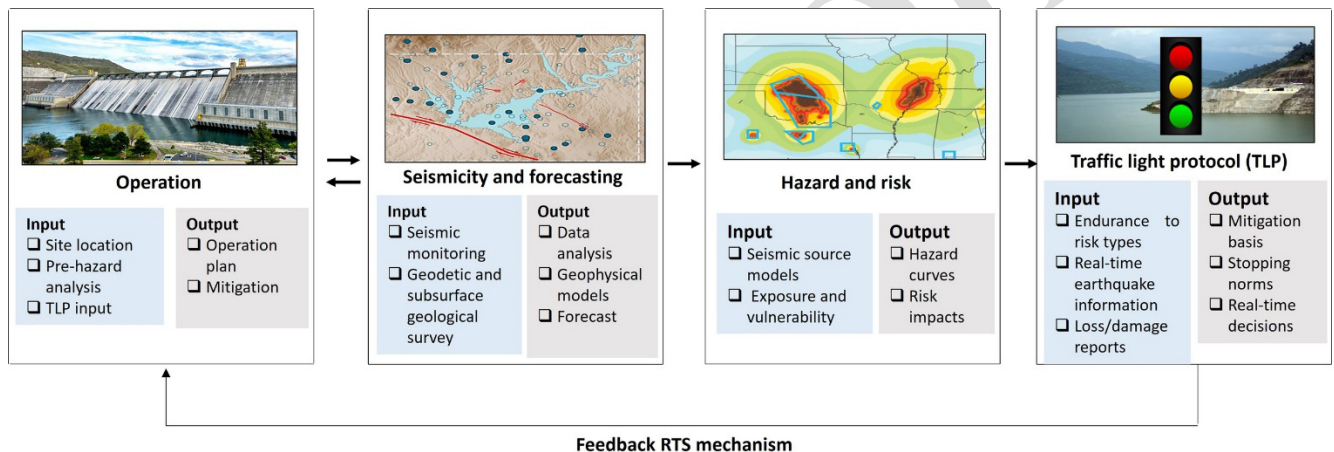
Figure 8. Reservoir operations and impoundment are strategically designed to reduce the risk of RTS. Monitoring seismic and geophysical activities yields information for predictive earthquake models. The catalogues of earthquakes and source/origin models are applicable in the assessment of hazard and risk. These assessments of risk and hazard can guide the development of a Traffic Light Protocol (TLP), functioning as a dynamic decision module during operations. Each box shows the classifications of input data (blue boxes) and output results (gray boxes).

utilization of physics-based models is promising, since they are capable of anticipating seismic activity, enabling operational adjustments for future mitigation of RTS risk (Boyet et al., 2023b) (Fig. 8).

Regarding the mitigation approaches for RTS within the framework of a TLP, the effectiveness of an operator heavily relies on the efficiency of mitigation strategies implemented at the yellow-light stage. Ideally, these strategies would proficiently diminish seismic risks and hazards, ultimately circumventing the red-light scenario that terminates the operation. Thus, TLPs can be one major strategy and strong decision-making tool for operators to minimize the risk of RTS for future developments of dams.

6 Conclusions

We have analyzed RTS at Irapé to discern the cause of the triggered seismicity. The measured low permeability of the rock at Irapé disregards pore pressure diffusion as the triggering mechanism and suggests that the $M_{3.0}$ RTS was triggered by the undrained response of the subsurface to reservoir impoundment. Analytical calculations estimate that pore

pressure increased by 0.61 MPa in response to an increase of 136 m in the reservoir water level. The resulting vertical effective stress increased by 0.75 MPa, and the horizontal effective stress increased by 0.48 MPa. Thus, the deviatoric stress would increase in a normal faulting stress regime, like the one at Irapé, destabilizing the fault and causing RTS. Both laboratory measurements and analytical calculations support the hypothesis that the initial seismicity was triggered by the undrained response of the subsurface to the loading of the reservoir at Irapé. This study suggests that the occurrence of such earthquakes may be avoided by thorough site characterization and careful management of the reservoir loading following TLPs that mitigate RTS risk.

Data availability. The data analyzed and/or used in this study are presented in the Supplement.

Supplement. The supplement related to this article is available online at: https://doi.org/10.5194/se-15-1-2024-supplement.

Author contributions. HR, GSF, and VV co-designed the study. ES and HR took samples and provided the map. HR wrote the paper and performed laboratory measurements. HR and VV did the analytical calculations. All authors reviewed the paper, contributed to the interpretation of the results, and edited the paper.

Competing interests. The contact author has declared that none of the authors has any competing interests.

Acknowledgements. This study was financed in part by the Coordenação de Aperfeiçoamento de Pessoal de Nível Superior -Brasil (CAPES)-Finance Code 001. The authors acknowledge funding from the Spanish National Research Council (CSIC) under the Program for Scientific Cooperation iCOOP+ through the Project COOPA20414. Victor Vilarrasa acknowledges funding from the European Research Council (ERC) under the European Union's Horizon 2020 research and innovation program through the Starting Grant GEoREST (https://www.georest.eu/, last access: 17 November 2024) under grant no. 801809. IMEDEA is an accredited "Maria de Maeztu excellence Unit" (grant no. CEX2021-001198, funded by MICIU/AEI/10.13039/501100011033). George Sand França gratefully acknowledges CNPq (grant no. 310240/2020-4 PQ-1C). George Sand França, Haris Raza, and Eveline Sayão also thank the INCTET-CNPq (Institutos Nacionais de Ciência e Tecnología de estudos tectónicos) Brazil. We thank Prof. Carlos Jorge de Abreu for conducting samples measurements at the Laboratory of Physical Properties of Rocks at the University of Brasília.

Financial support. This research has been supported by the Coordenação de Aperfeiçoamento de Pessoal de Nível Superior (Finance Code 001), the Consejo Superior de Investigaciones Científicas (grant no. COOPA20414), the EU H2020 European Research Council (grant no. 801809), the Consejo Superior de Investigaciones Científicas (grant no. CEX2021-001198, funded by MCIN/AEI/10.13039/501100011033), and the Conselho Nacional de Desenvolvimento Científico e Tecnológico (grant no. 310240/2020-4 PQ-1C).

The article processing charges for this open-access publication were covered by the CSIC Open Access Publication Support Initiative through its Unit of Information Resources for Research (URICI).

Review statement. This paper was edited by Simone Pilia and reviewed by Sarah Weihmann and one anonymous referee.

References

Almeida, F. F. M.: The São Francisco Craton, Brazilian Journal of Geosciences, 7, 349–364, 1977.

API: Recommend Practices for Core Analysis, RP40, American Petroleum Institute, 2nd Edition, https://energistics.org/sites/default/files/2022-10/rp40.pdf (last access: 17 November 2024), 1998.

Araujo Filho, J. O., Silva, G. F., Lima, E. A. M., Ferreiara, V. N., Batista, O. C. A., and Franca, G. S.: Mapeamento Geoestrutural da área de influência da Usina Hidrelétrica de Irapé, Grão Mogol, MG, Anais do 45° Congresso Brasileiro de Geologia, Sociedade Brasileira de Geologia, https://doi.org/10.22564/5simbgf2012.160, 2010.

Arora, K., Srinu, Y., Gopinadh, D., Chadha, R. K., Raza, H., Mikhailov, V., Ponomarev, A., Kiseleva, E., and Smirnov, V.: Lineaments in Deccan Basalts: The Basement Connection in the Koyna–Warna RTS Region, Bull. Seismol. Soc. Am., 108, 2919–2932, https://doi.org/10.1785/0120180011, 2018.

Assumpçao, M., James, D., and Snoke, A.: Crustal thicknesses in SE Brazilian Shield by receiver function analysis: Implications for isostatic compensation, J. Geophys. Res., 107, ESE 2-1–ESE 2-14, https://doi.org/10.1029/2001JB000422, 2002.

Assumpção, M., Feng, M., Tassara, A., and Julia, J.: Models of crustal thickness for South America from seismic refraction, receiver functions and surface wave tomography, Tectonophysics, 609, 82–96, 2012.

Bell, M. L. and Nur, A.: Strength changes due to reservoir-induced pore pressure, stresses, and application to Lake Oro-Berrocal, J. Geophys. Res., 83, 4469–4483, 1978.

Bondarenko, N., Podladchikov, Y., and Makhnenko, R.: Hydromechanical impact of basement rock on injection-induced seismicity in Illinois Basin, Sci. Rep., 12, 15639, https://doi.org/10.1038/s41598-022-19775-4, 2022.

Boyet, A., De Simone, S., Ge, S., and Vilarrasa V.: Poroelastic stress relaxation, slip stress transfer and friction weakening controlled post-injection seismicity at the Basel Enhanced Geothermal System, Commun. Earth Environ., 4, 104, https://doi.org/10.1038/s43247-023-00764-y, 2023a.

Boyet, A., De Simone, S., and Vilarrasa, V.: Physics-Based Modeling to Understand and to Propose Forecasting Methods of Induced Seismicity, Seismol. Res. Lett., 94, 2666–2678, https://doi.org/10.1785/0220230109, 2023b.

Carder, D. S.: Seismic investigation in the Boulder Dam area, 1940–1944, and the influence of reservoir loading on earthquake activity, B. Seismol. Soc. Am., 35, 175–192, 1945.

Ceia, M., Missagia, R., Fasolo, R., and Neto, I. L.: Relationship between porosity, permeability, and pore compressibility, https://doi.org/10.22564/16cisbgf2019.287, 2019.

Cesca, S., Braun, T., Maccaferri, F., Passarelli, L., Rivalta, E., and Dahm, T.: Source modelling of the M5–6 Emilia-Romagna, Italy, earthquakes (2012 May 20–29), Geophys. J. Int., 193, 1658–1672, https://doi.org/10.1093/gji/ggt069, 2013.

Cesca, S., Grigoli, F., Heimann, S., González, Á, Buforn, E., Maghsoudi, S., Blanch, E., and Dahm, T.: The 2013 September–October seismic sequence offshore Spain: a case of seismicity triggered by gas injection?, Geophys. J. Int., 198, 941–953, https://doi.org/10.1093/gji/ggu172, 2014.

Chen, L. and Talwani, P.: Mechanism of initial seismicity following impoundment of the Monticello Reservoir, South Carolina, B. Seismol. Soc. Am., 91, 1582–1594, 2001.

Chimpliganond, C., França, G. S., Bandeira, A. E., and Bevilaqua, L.: Reservoir-triggered seismicity at the highest Brazilian dam, AGU 2007 – Meeting of Americas Joint Assembly Abstract, Acapulco, Mexico, Acapulco, Mexico, 22–25 May, https://ui.adsabs.harvard.edu/abs/2007AGUSM.S51B.03C/abstract (last access: 18 November 2024), 2007.

Cocco, M. and Rice, J. M.: Pore pressure and poroelasticity effects in Coulomb stress analysis of earthquake interactions, J. Geophys. Res., 107, 2069, https://doi.org/10.1029/2000JB000138, 2002.

Ellsworth, W. L.: Injection-induced earthquakes, Science, 341, 1225942, https://doi.org/10.1126/science.1225942, 2013.

Foulger, G. R., Wilson, M., Gluyas, J., Julian, B. R., and Davies, R.: Global review of human-induced earthquakes, Earth-Sci. Rev., 178, 438–514, 2018.

França, G. S., Assumpção, M., Ribotta, L. C., Von Huelsen, M. G., and Chimpliganond, E. C. N.: Updated compilation of reservoir triggered seismicity in Brazil, in 2010 The Meeting of the Americas (AGU – American Geophysical Union), Foz do Iguaçu, Paraná, Brazil, https://repositorio.usp.br/item/002193775 (last access: 18 November 2024), 2010.

González, P. J., Tiampo, K. F., Palano, M., Cannavó, F., and Fernández, J.: The 2011 Lorca earthquake slip distribution controlled by groundwater crustal unloading, Nat. Geosci., 5, 821–825, https://doi.org/10.1038/ngeo1610, 2012.

Golstein, P. and Snoke, A.: Sac Avaliability for the Iris Community, Incorporated Institutions for Seismology Data Management Center Eletronic Newsletter, https://www.scirp.org/reference/referencespapers?referenceid=1195449 (last access: 15 December 2013), 2005.

Grigoli, F., Cesca, S., Rinaldi, A. P., Manconi, A., López, Comino, J. A., Clinton, J. F., Westaway, R., Cauzzi, C., Dahm, T., and Wiemer, S.: The November 2017 M_w 5.5 Pohang earthquake: a possible case of induced seismicity in South Korea, Science, 360, 1003–1006, https://doi.org/10.1126/science.aat2010, 2018.

Gupta, H. K.: A review of recent studies of triggered earthquakes by artificial water reservoirs with special emphasis on earthquakes in Koyna, India, Earth-Sci. Rev. 58, 279–310, doi.org/10.1016/S0012-8252(02)00063-6, 2002.

Gupta, H. K., Arora, K., Purnachandra Rao, N., Roy, S., Tiwari, V. M., Patro, P. K., Satyanarayana, H. V. S., Shashidhar, D., Mahato, C. R., Srinivas, K. N. S. S. S., Srihari, M., Satyavani, N., Srinu, Y., Gopinadh, D., Raza, H., Jana, M., Akkiraju, V. V., Goswami, D., Vyas, D., Dubey, C. P., Raju, D. C. V., Borah, U., Raju, K., Chinna Reddy, K., Babu, N., Bansal, B. K., and Nayak, S.: Investigations of continued reservoir triggered seismicity at Koyna, India, Geol. Soc. Lond. Spec. Publ., 445, 151–188, 2016.

Keranen, K. M., Savage, H. M., Abers, G. A., and Cochran, E. S.: Potentially induced earthquakes in Oklahoma, USA: Links between wastewater injection and the 2011 M_w 5.7 earthquake sequence, Geology, 41, 699–702, 2013.

Keranen, K. M., Weingarten, M., Abers, G. A., Bekins, B. A., and Ge, S.: Sharp increase in central Oklahoma seismicity since 2008 induced by massive wastewater injection, Science, 345, 448–451, https://doi.org/10.1126/science.1255802, 2014.

Kim, K.-H., Ree, J.-H., Kim, Y., Kim, S., Kang, S. Y., and Seo, W.: Assessing whether the 2017 M_w 5.4 Pohang earthquake in South Korea was an induced event, Science, 360, 1007–1009, https://doi.org/10.1126/science.aat6081, 2018.

Kivi, I. R., Boyet, A., Wu, H., Walter, L., Hanson-Hedgecock, S., Parisio, F., and Vilarrasa, V.: Global physics-based database of injection-induced seismicity, Earth Syst. Sci. Data, 15, 3163–3182, https://doi.org/10.5194/essd-15-3163-2023, 2023.

Lee, W. H. K., and Lahr, J. C.: HYPO 1971 (revised a computer program for determining hypocentre, magnitude and first motion pattern of local earthquakes. USGS, Open file report, 64 pp., https://doi.org/10.3133/ofr75311, 1975.

Lima, S. A. A., Martins-Neto, M. A., Predrosa-Soares, A. C., Cordani, U. G., and Nutman, A.: The Salinas Formation in the Type Area, NE of Minas Gerais: a proposal to review the stratigraphy of the Araçuaí Belt based on sedimentary and metamorphic evidence and U-Pb SHRIMP ages, Braz. J. Geosci., 34, 491–500, 2002.

Marshak, S., Alkmim, F. F., Whittington, A., and Pedrosa-Soares, A. C.: Extensional collapse in the Neoproterozoic Araçuaí orogen, eastern Brazil: a setting for reactivation of asymmetric crenulation cleavage., J. Struct. Geol., 28, 129–114, 2006.

McGarr, A., Simpson, D., and Seeber, L.: 40 – Case Histories of Induced and Triggered Seismicity, Int. Geophys., 81, 647–661, https://doi.org/10.1016/s0074-6142(02)80243-1, 2002.

Neuzil, C. E.: Groundwater flow in low-permeability environments, Water Resour. Res., 22, 1163–1195, 1986.

Raza, H., Kivi, I. R., França, G. S., and Vilarrasa V.: Reservoir impoundment-triggered seismicity in Brazil: the case of M4.0 Nova Ponte earthquake, Sci. Rep., 13, 22226, https://doi.org/10.1038/s41598-023-48924-6, 2023.

Rice, J. R. and Cleary, M. P.: Some basic stress-diffusion solutions for fluid-saturated elastic porous media with compressible constituents, Rev. Geophys. Space Ge., 14, 227–241, 1976.

Roeloffs, E. A.: Fault stability changes induced beneath a reservoir with cyclic variations in water level, J. Geophys. Res., 93, 2107–212, 1988.

Rutqvist, J.: The geomechanics of CO_2 storage in deep sedimentary formations, Geotechnical and Geological Engineering, 30, 525–551, 2012.

Sayão, E., França, G. S., Holanda, M., and Gonçalves, A.: Spatial database and website for reservoir-triggered seismicity in Brazil, Nat. Hazards Earth Syst. Sci., 20, 2001–2019, https://doi.org/10.5194/nhess-20-2001-2020, 2020.

Silva, G. F., Araújo Filho, J. O., Von Huelsen, M. G., Chimpliganond, C. N., and França, G. S.: Influence of Brazilian structures on the reservoir-induced seismicity case of Irapé Hydroelectric Plant, Minas Gerais, Brazil, Braz. J. Geol., 44, 375–386, https://doi.org/10.5327/Z2317-4889201400030004, 2014.

Simpson, D. W.: Seismicity change associated with the reservoir loading, Eng. Geol., 10, 123–150, 1976.

Simpson, D. W., Leith, W. S., and Scholz, C. H.: Two types of reservoirs induced seismicity, B. Seismol. Soc. Am., 78, 2025–2040, 1988.

Skempton, A. W.: The pore-pressure coefficients *A* and *B*, Geotechnique, 4, 143–114, 1954.

Talwani, P. and Acree, S.: Pore pressure diffusion and mechanism of reservoir induced seismicity, Pure Appl. Geophys., 122, 947–965, 1985.

Vilarrasa, V., Carrera, J., Olivella, S., Rutqvist, J., and Laloui, L.: Induced seismicity in geologic carbon storage, Solid Earth, 10, 871–892, https://doi.org/10.5194/se-10-871-2019, 2019.

Vilarrasa, V., De Simone, S., Carrera, J., and Villaseñor, A.: Unravelling the causes of the seismicity induced by underground gas storage at Castor, Spain, Geophys. Res. Lett., 48, e2020GL092038, https://doi.org/10.1029/2020GL092038, 2021.

Vilarrasa, V., De Simone, S., Carrera, J., and Villaseñor, A.: Multiple induced seismicity mechanisms at Castor underground gas storage illustrate the need for thorough monitoring, Nat. Commun., 13, 3447, https://doi.org/10.1038/s41467-022-30903-6, 2022.

Vilarrasa, V., Raza, H., Kivi, I. R., and França, G. S.: Understanding the triggering mechanisms of reservoir-triggered seismicity at Nova Ponte, Brazil, through hydro-mechanical modeling, EGU General Assembly 2023, Vienna, Austria, 24–28 Apr 2023, EGU23-11711, https://doi.org/10.5194/egusphere-egu23-11711, 2023.

Wilson, M. P., Foulger, G. R., Gluyas, J. G., Davies, R. J., and Julian, B. R.: HiQuake: The Human-Induced Earthquake Database, Seismol. Res. Lett., 88, 1560–1565, https://doi.org/10.1785/0220170112, 2017.

Yeck, W. L., Weingarten, M., Benz, H. M., McNamara, D. E., Bergman, E. A., Herrmann, R. B., Rubinstein, J. L., and Earle, P. S.: Far-field pressurization likely caused one of the largest injections induced earthquakes by reactivating a large preexisting basement fault structure, Geophys. Res. Lett., 43, 10198–10207, https://doi.org/10.1002/2016GL070861, 2016.